A Novel Marine Radar Targets Extraction Approach Based on Sequential Images and Bayesian Network

Feng Ma[1, 2, 3, 4], Yu-wang Chen[2], Xin-ping Yan[1, 3], Xiu-min Chu[1, 3], Jin Wang[4]
Intelligent Transport System Research Center, Wuhan University of Technology, P.R. China[1]
Decision and Cognitive Sciences Research Centre, the University of Manchester, Manchester M15 6PB, UK[2]
National Engineering Research Center of Water Transportation Safety (WTS), P. R. China[3]
Liverpool Logistics, Offshore and Marine (LOOM) Research Institute, Liverpool John Moores University, L3 3AF, UK[4]

Abstract: This research proposes a Bayesian Network-based methodology to extract moving vessels from a plethora of blips captured in frame-by-frame radar images. First, the inter-frame differences or graph characteristics of blips, such as velocity, direction, and shape, are quantified and selected as nodes to construct a Directed Acyclic Graph (DAG), which is used for reasoning the probability of a blip being a moving vessel. Particularly, an unequal-distance discretisation method is proposed to reduce the intervals of a blip's characteristics for avoiding the combinatorial explosion problem. Then, the undetermined DAG structure and parameters are learned from manually verified data samples. Finally, based on the probabilities reasoned by the DAG, judgments on blips being moving vessels are determined by an appropriate threshold on a Receiver Operating Characteristic (ROC) curve. The unique strength of the proposed methodology includes laying the foundation of targets extraction on original radar images and verified records without making any unrealistic assumptions on objects' states. A real case study has been conducted to validate the effectiveness and accuracy of the proposed methodology.

Keywords: Marine Radar; Bayesian Network; Continuous Attribute Discretisation; Evidence Distance; Targets Extraction

1 Introduction and background

Marine radar is the most important sensor for navigation or port management, as in practice it is capable of detecting vessels, waterfronts, and rocks actively. In an efficient form of perception, a marine radar system offers sequential images, which mark vessels or other objects as blips on screen. Moreover, the dynamic characteristics of blips can also be measured through Doppler velocities. However, most marine radar systems work on a low Repetition Pulse Frequency (RPF) mode and the Doppler velocities are often ambiguous. Since radar images are the kernel evidence of target extraction, many marine radar systems incorporate Automatic Radar Plotting Aid (ARPA) functions to identify and track moving blips automatically with green circles reminding operators of potential moving vessels. As a special type of marine radar, the coastal surveillance radar is even capable of tracking more than 1,000 blips simultaneously with the support of an effective ARPA function. Generally, a conventional ARPA function is designed from filtering algorithms, which are formulated for extracting actual trajectories of blips (Kosuge *et al.*, 1997).

Presently, ARPA radar plays an essential role in the estimation of collision risk. Goerlandt *et al.* (2015) described the risks in collision alert system (CAS) applications, and proposed a novel framework for maritime risk-informed CAS. Simsir *et al.* (2014) investigated the CAS in complex fairways. Chin and Debnath (2009) proposed a new method to perceive collision risk in a port waterway. In their research, ARPA radar is used as the major sensor for tracking vessels, and the collision risk estimation is generally based on the information obtained from ARPA targets. Problematic ARPA information might trigger false alerts.

In recent years, marine radar has been improved rapidly, especially in terms of the sensitivity and ability of noise suppression. The latest S band marine radar is capable of tracking a $0.5m^2$ target 5 miles away. Obviously, radar systems with high sensitivity provide more informative images of surroundings. On the other hand, high quality images generally bring a plethora of blips or objects, which might confuse operators. A $0.5m^2$ target shown as a blip can be a canoe, a drowning person, a sea weed, a background noise, or even a lump of trash floating on the water. However, the ARPA function is not capable of distinguishing their differences. Therefore, in the harbour management and the CAS systems discussed previously, supervisors always have to identify moving vessels from hundreds of ARPA targets and blips manually. In other words, how to identify them effectively becomes an important issue related to safety. Meanwhile, ship crews and vessel traffic service (VTS) supervisors also have to identify banks, shoals, rocks and channel structures in order for them to avoid possible grounding and collision incidents with harbour facilities (Mazaheri *et al.*, 2014; Nam *et al.*, 2015).

In fact, supervisors are often able to identify the authenticity of a blip by further inspecting its graph and motion characteristics. However, the identification will cost a supervisor a certain amount of time. In busy waterways, such one-by-one inspections from too many blips become impractical. For instance, in Nantong Waterway of Yangtze River, China, there are about 20,000 vessels passing through each day. Therefore, it is impossible to ensure that all the blips are inspected manually. A realistic solution is to simulate such human intelligence to extract moving vessels from blips automatically. Referring to manual work, this intelligence does not require precise speeds, courses or trajectories of blips. Another challenge for marine radar targets extraction is uncertainty. Weather conditions and observation angles will change the graph of a blip notably. Since the resolution of radar is limited, the moving trajectories of blips are always different from the actual ones and they are often unstable. Moreover, multiple blips overlap with or connect to each other frequently, making the direct identification difficult. Therefore, the key issue is to address the uncertainties associated with the sequential radar images. In practice, a blip caused by background noise might drift with a steady speed which is similar to a moving vessel, whilst a real moving vessel might hold an extremely low speed to approach a berth, and it looks like a stationary noise. In other words, the differences between moving vessel blips and other ones are not distinctive.

In practice, radar operators often take consideration of several characteristics simultaneously to make their judgments. To build this artificial intelligence, an ideal approach should be capable of making conjunctive inference with several characteristics of blips under uncertainties. In fact, a number of methods have already been introduced into radar research, such as Dempster's rule (Li and Pang, 2013; Dempster, 1967), neural network (Shafiei and Binazadeh, 2015) and fuzzy cluster (Ma *et al.*, 2015). The human experience mentioned above can be considered as a kind of prior information in probabilistic inference. As an efficient probabilistic inference tool to model uncertainty, Bayesian Network (BN) is widely considered to be superior and rigorous (Zhang *et al.*, 2013). Montewka *et al.* (2015) used a BN-based probabilistic model to predict a ship performance in dynamic ice. Hänninen and Kujala (2014) proposed Bayesian network models for Port State Control studies. Goerlandt and Montewka (2014) used a BN-based model for estimating accidental cargo oil outflow from product tankers in a ship-ship collision.

The research is aiming to propose a BN-based identification methodology to extract moving vessels from radar blips based on the inter-frame differences and graph characteristics. The remainder of this paper is organised as follows. In Section 2, radar image characteristics, conventional filtering and classification methods are introduced. Section 3 presents a BN-based targets extraction methodology. In Section 4, a case study is conducted to demonstrate and validate the proposed methodology. The paper is concluded in Section 5.

2 Conventional radar targets extraction methods

The ARPA function of marine radar is initially designed for collision avoidance, which does not concern the authenticity, importance or behaviour of blips (Yoo and Kim, 2003). Presently, in a busy waterway, pattern recognition of vessel behaviours becomes increasingly important, especially for port management (Riveiro *et al.*, 2008). In this section, typical identification methods in radar image research are briefly reviewed.

2.1 The uncertainties in radar images

Radar echo signals can be visualised as blips on screen. In such a form, the radar formulates the surroundings as a grey-scale image, or a pseudo-colour image, and each pixel in radar images generally represents the echo intensity. For example, the satellite image and the grey-scale radar image are shown in Figure 1 respectively, which capture the same location and surroundings of Yangtze River, Zhutuo County, Chongqing, China. The radar image is obtained from the maritime radar belonging to the local administration, while the satellite image is obtained from the Google map. The position of radar is marked as a five-point star in both images. With the help of the radar image on the right-hand side, radar operators are able to differentiate the vessels, waterfronts, and bridges. However, much information is missing in the radar image. First of all, an area is blocked and marked as 'Blind Area', and it cannot be observed. Secondly, the 'Shoal and Rock' marked in the satellite image is shown as stationary blips, which are quite similar to vessels. Moreover, some blips marked as 'Random Noise' are moving like vessels, but they are most likely to be caused by multi-path effects or background noises.

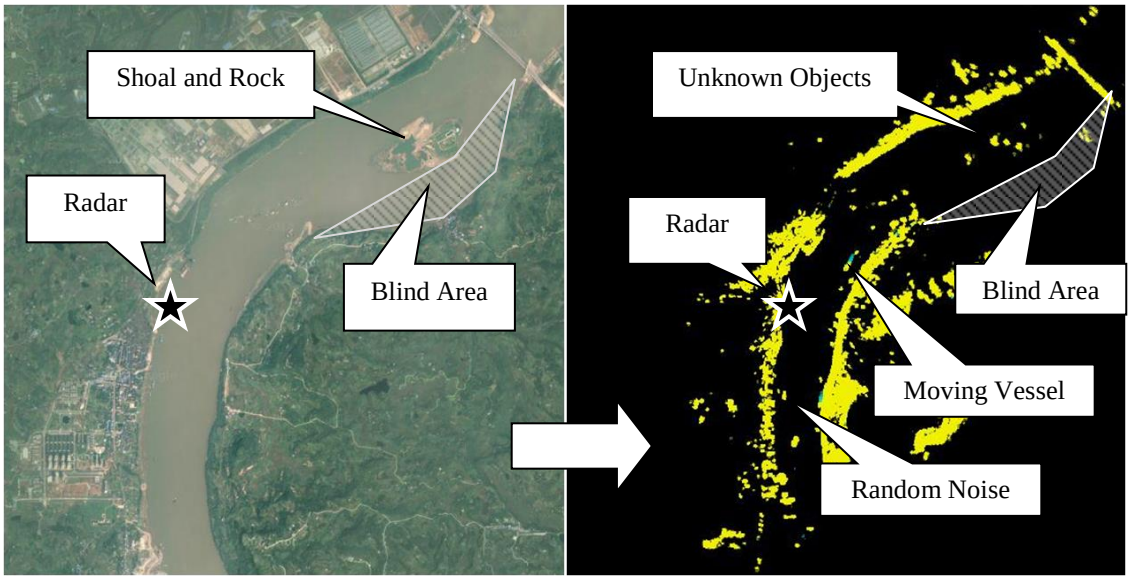

Figure 1 The satellite and grey-scale radar image of Yangtze River, Chongqing, China

Using binarization and segmentation algorithms, a radar image can be divided into a group of colour spots or blips with different shapes and sizes, which indicate different kinds of objects (Ranjani and Thiruvengadam, 2012). The following problem is to identify such blips or objects. In other types of radar, the pattern differences can be found in the frequency spectrum characteristics of blips, especially for Synthetic Aperture Radar (SAR). Carvalho *et al.* (2010) proposed a SAR imagery segmentation method by statistical region growing and hierarchical merging. Chen (2015) proposed a novel method to distinguish low-altitude targets from sea clusters with the spatial and temporal features of the radar image sequence. For marine radar, Vicen-Bueno *et al.* (2009) proposed an approach to reduce the influence of sea clusters. In practice, operators are generally able to identify the blips correctly, simply based on blips' graphic characteristics rather than frequency spectrums.

2.2 Filtering and classification methods on radar objects

As discussed previously, trajectories captured by blips are doubtful, which are illustrated in Figure 2. In the figure, the centres of a cargo vessel named object 26 are represented with white dots, and they can be connected with a solid zigzag line, which is presented as the captured trajectory on the right-hand side of Figure 2. Obviously, it is impossible for this cargo vessel to move in such a strange trajectory. It is more likely to keep a stable direction. Therefore, it can be assumed that the object was moving in an approximately linear manner. With appropriate radar filtering algorithms, a linear trajectory can be found, which is represented as a dash line on the right-hand side of Figure 2. In high speed monitoring, especially for aircrafts or missiles, such assumptions and algorithms are reasonable and efficient (Farrell, 2008; He *et al.*, 2015).

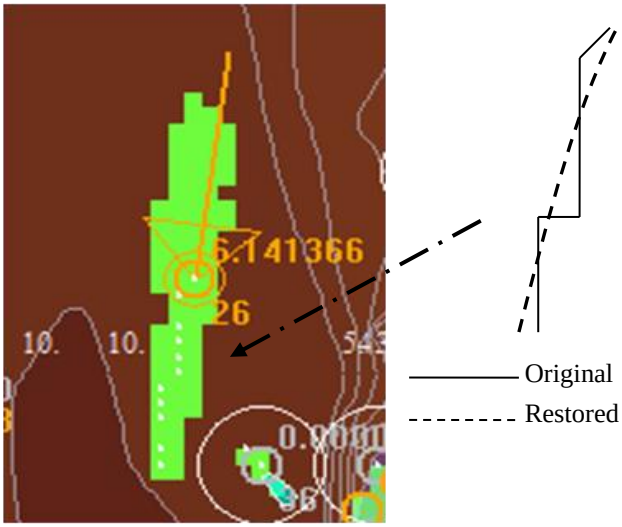

Figure 2 Original Trajectory of Object 26 (cargo) observed by radar

The typical radar filtering algorithms include the least square algorithm, α-β filter, α-β-ϒ filter, extended Kalman filter, and particle filter. Yoo and Kim (2003) proposed an algorithm named α–β–Λ which incorporates an estimation technique of the tracking index. He *et al.* (2015) designed the IMM-UKF-UPF algorithm which combines the Unscented Kalman Filter (UKF) algorithm with the Unscented Particle Filter (UPF) algorithm to reduce the influence of flicker noises for ground-based radar. De Feo *et al.* (1997) compared MHT and IMM-JPDA with Kalman filtering in radar tracking. However, assumptions on the status of objects and noises have to be made in all the filtering algorithms. For marine radar, the differences between noise objects and real moving vessels are not distinctive as discussed previously. Therefore, by now, the marine radar ARPA function based on α-β

filter is only practical in the open sea. Moreover, due to such assumptions, the values of dynamic attributes offered by ARPA functions are not accurate (IEC, 2013).

To address the problem that radar captures false targets, researchers have introduced several classification algorithms to identify them. For marine radar, Ma *et al*. (2015) proposed a classification method to identify the false ARPA targets using fuzzy k-means (FCM), and the reported accuracy is 91.0%. However, the question is that the dynamic attributes of ARPA targets are not fully reliable. As a result, the classification is not completely credible. More research was conducted in other types of radar. Zhou *et al.* (2013) invented a radar target recognition method based on fuzzy optimal transformation using high-resolution range profiles. This method can be used to maximize the between-class distance, while preserving the within-class structure. Zhai and Jiang (2014) developed a novel method to detect and classify targets based on real data collected from a bistatic ultra-wideband (UWB) radar system and using a developed target type classification and recognition algorithm. Zhao *et al*. (2014) invented a hierarchical vessel classifier based on k-Nearest Neighbors (KNN) algorithm for high-resolution inverse SAR images. All the above classifiers or pattern recognition methods did not fully take the uncertainties of radar images into consideration, although they are efficient in specific applications.

3 A proposed methodology

This research proposes a novel radar extraction or classification methodology to simulate manual work based on probabilistic inference. The flow of this methodology is illustrated in Figure 3. At first, several inter-frame differences or attributes of radar blips are quantified. Then, to avoid the combinatorial explosion, a new method is proposed to discretise the original intervals of these attributes. Subsequently, these attributes and the authenticity of blips are used to construct a new DAG to reason the probability of a blip being a real moving vessel. Eventually, based on the probabilities reasoned by the DAG, final judgements on if a blip is a moving vessel can be made using a receiver operating characteristic (ROC) curve.

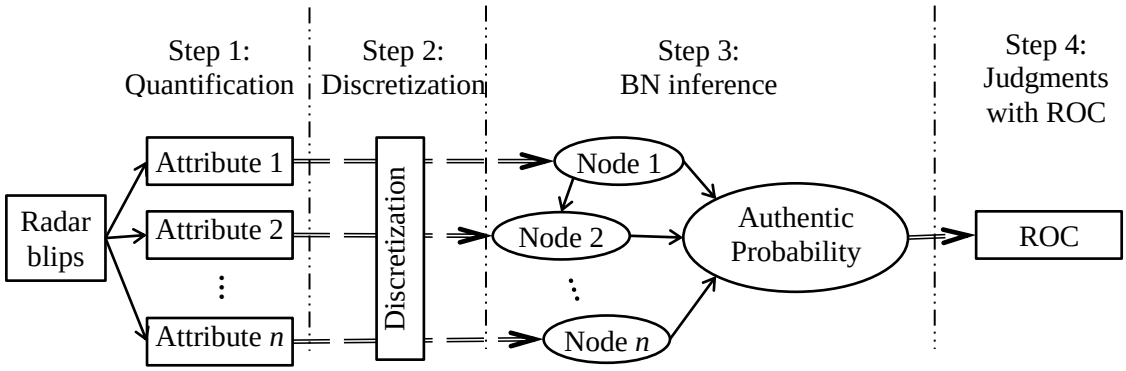

Figure 3 The flow of the proposed methodology

3.1 Step 1: Radar image inter-frame differences quantification

Operators are able to distinguish objects using the inter-frame differences and graphic characteristics, including velocity, course, size, colour, width and length of blips. The prominent advantage of BN is that the dependencies among all the factors can be modelled properly (Zhang *et al.*, 2013). Therefore, under the framework of BN, all the characteristics above can be included to conduct conjunctive inference. To simplify the model, three pieces of key evidence (*i.e.*, attributes) are selected

in this research which are velocity, motion direction, and blip shape (*i.e.*, slenderness) respectively, as shown in Figure 4.

Referring to manual work and the ARPA function requirements (IEC, 2013), operators are generally able to identify the targets in 25 seconds, or 10 continuous frames. Therefore, this research extracts the velocity and direction characteristics from an analysis of 10 frames. In the future research, fewer frames could be considered.

Generally, moving vessels are more likely to sail with a steady speed and a steerable course. On contrary, noise objects are more likely to drift around small areas. Hence, the velocity and motion course can be quantified as illustrated in Figure 4. In the figure, the original sequential images have been casted on an electronic chart after binarization. Then, the centres of radar blips are marked as white dots in sub-figure 4(e). When connecting the centres of a radar blip in adjacent frames, an initial radar trajectory can be obtained as illustrated in sub-figure 4(d). The velocity of the radar blip equals to the number of units (pixels) that the blip has moved in 10 frames, or the displacement. The direction is quantified as the "included angle" between the true north and the motion direction, which is illustrated in sub-figure 4(b). For simplicity, all the values above are rounded down to integers.

Intuitively, according to the images, a moving vessel's blip is more slender than a noise's, and the principle is illustrated in Figures 2 and 4. This is because the imagery delay is a common function of radar with moving blips possessing afterglows. Therefore, the slenderness of a blip can be considered as a distinctive graph characteristic, which can be computed as the quotient of a blip's pixel size (S_2) to blip circumcircle area (S_1). This process is illustrated in sub-figure 4(c), where S_2/S_1 is defined as the slenderness.

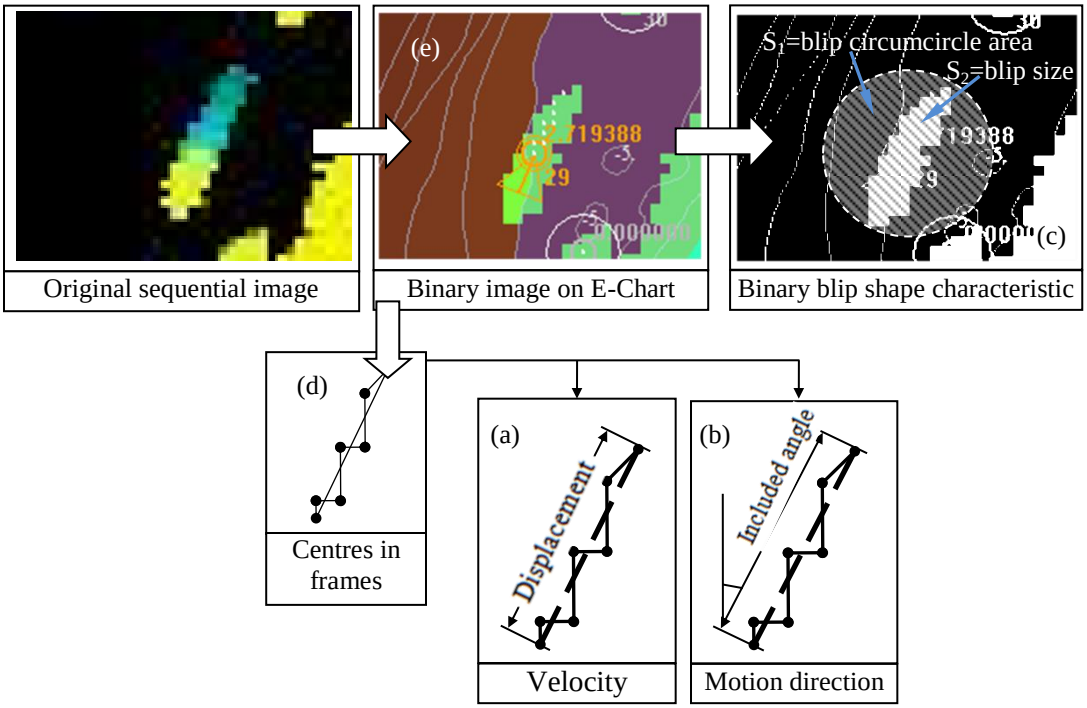

Figure 4 Blip characteristics in frames of radar

3.2 Step 2: Unequal-distance discretisation optimisation

After appropriate binarization and segmentation algorithms have been used, the velocity, direction and shape (slenderness) are quantified. Before inference, the observation (measurement) values obtained from graph characteristics and dynamic attributes need further discretisation;

otherwise there will be a combinatorial explosion problem. Taking vessel speed as an example, the speed values between 0 and 30.0 knots are considered to be meaningful. As a result, there will be 300 hundred exclusive observation values when taking the interval size of 0.1 knots. Generally speaking, a smaller interval in discretisation makes the model closer to the reality. However, smaller intervals will increase the complexity, especially in modelling of the joint probabilities in a BN.

Much work has been conducted to find optimal intervals in continuous observations, including entropy methods, the Adaptive Discretisation Intervals (ADI) method and the Minimum Descriptive Length (MDL) method (Kotsiantis and Kanellopoulos, 2006; Clarke and Barton, 2000). Entropy methods are based on Shannon Entropy that is an accurate measurement on the amount of information. An optimal interval can be solved in the trade-off between the entropy value and the complexity. However, Shannon Entropy is a theoretical boundary value. All the entropy measurement methods are just similar to Shannon Entropy. Moreover, the optimisation of intervals is generally conducted on equal-distance discretisation, which might not provide an optimal solution. Different from entropy methods, the MDL method is applied for global optimisation, which combines a measure of the underlying probability distributions of the data sample with a consideration of the network complexity (Grünwald, 2000). Compared with others, the ADI method is more relevant to heuristic methods, which can only be applied under specific assumptions on the distribution (Bacardit and Garrell, 2003).

In this research, an un-equal distance discretisation method is proposed. In fact, quantified characteristics of blips are discrete as described in Section 3.1. Therefore, the discretisation is indeed a merging operation, which will reduce the number of original intervals and simplify the inference. Simultaneously, such a merging will cause a loss of original information. To find an optimal discretisation, the key issue is to quantify this loss.

3.2.1 Likelihood modelling

The velocity, direction and slenderness can be considered as three different pieces of evidence to reason the authenticity of a blip. In other words, the values of the attributes above can be mapped as probabilities or likelihoods of authenticity. Suppose $\Theta = \{\theta_{True}, \theta_{False}\}$ is a set of mutually exclusive and collectively exhaustive propositions for recognitions of blips, where θ_{True} is a True state and θ_{False} a False state. Let Ø represent the empty set. Then, Θ is referred to as a frame of discernment. A *Basic Probability Assignment* (*bpa*) is a function *p*: $2^{\Theta} \rightarrow [0,1]$ that satisfies,

$$p(\varnothing) = 0, \sum_{\theta \subseteq \Theta} p(\theta) = 1 \quad (1)$$

where the basic probability $p(\theta)$ is assigned exactly to a proposition θ and not to any smaller subset of θ. $p(\theta)$ can be generated from the values of attributes, including the velocity, direction or slenderness of a blip. Referring to the research conducted by Yang and Xu (2014), the likelihoods of authenticity based on observation values can be presented below.

Let $V = \{v_1, v_2, \cdots, v_K\}$ be the *K* measurement values observed from a blip's individual attribute (Xu *et al.*, 2013), which can be the velocity, direction, or slenderness. In historical data, the observations from the verified objects of the False state are denoted by $Q^0 = \{q^0_{v_1}, q^0_{v_2}, \cdots, q^0_{v_K}\}$ with the sample size S^0, and $q^0_{v_i}$ denotes the frequency or amount of a singleton measurement value v_i in the observations of the False state (noise or stationary). Similarly, the observations from the verified

objects of the True state are denoted by $Q^1 = \{q^1_{v_1}, q^1_{v_2}, \cdots, q^1_{v_K}\}$ with the sample size S^1, and $q^1_{v_i}$ denotes the frequency or amount of a singleton measurement value v_i in the observations of the True state (moving vessels). These two sets of observations are shown in Table I.

Table I. Radar Observations

Verified sample	Radar observation attribute values in the hypotheses					
	sample size	v_1	⋯	v_i	⋯	v_K
False state (0)	S^0	$q^0_{v_1}$	⋯	$q^0_{v_1}$	⋯	$q^0_{v_1}$
True state (1)	S^1	$q^1_{v_1}$	⋯	$q^1_{v_i}$	⋯	$q^1_{v_K}$

In the discrimination framework $\{False(0), True(1)\}$, each $c^j_{v_i}$ stands for the likelihood of the hypothesis *j* state when v_i is captured, which is presented in Eq. (2) and Table II:

$$c^j_{v_i} = q^j_{v_i} / S^j, \text{ for } i = 1, \ldots, K, \quad j = 0, 1. \tag{2}$$

Table II. Likelihoods

Hypotheses	Radar observation attribute values' likelihoods in the hypotheses				
	v_1	⋯	v_i	⋯	v_K
False state (0)	$c^0_{v_1}$	⋯	$c^0_{v_i}$	⋯	$c^0_{v_K}$
True state (1)	$c^1_{v_1}$	⋯	$c^1_{v_i}$	⋯	$c^1_{v_K}$

If all observations in Table I are conducted independently, the relationship between likelihood $c^j_{v_i}$ and probability (normalised likelihood) $p^j_{v_i}$ is given by (Yang and Xu, 2014),

$$p^j_{v_i} = c^j_{v_i} / (c^0_{v_i} + c^1_{v_i}), \text{ for } i = 1 \ldots K, j = 0, 1. \tag{3}$$

Using Eq. (3), v_i can be mapped to likelihoods of authenticity (the True or False state), or a relative likelihood vector $\vec{p}_{v_i} = \{p^0_{v_i}, p^1_{v_i}\}$, where 0 denotes the False state, and 1 denotes the True state.

3.2.2 Discretisation modelling with buckets

As discussed, taking original observation values as intervals (discrete states) in BN modelling is not appropriate, which might lead to combinatorial explosion. To reduce the intervals of a single attribute or node in BN modelling, some consecutive observation (measurement) values have to be merged together as a new interval. This merging will cause information losses. With the help of likelihood vectors, such losses can be quantified and described as follows.

As shown in Figure 5 and Table I, for the *K* individual original observation (measurement) values $\{v_1, \cdots, v_K\}$, their likelihood vectors $\{\vec{p}_{v_1}, \cdots, \vec{p}_{v_K}\}$ can be computed with Eqs. (2) and (3). To reduce the number of intervals in BN modelling, these original observation values have to be merged to *L* buckets as shown in Figure 5. A bucket here denotes a set of consecutive observation values, or an interval after merging. In this figure, the consecutive observation values between two adjacent bold lines are merged into a bucket. Let I_l denote the number of consecutive observation values which fall into the l^{th} bucket, hence $\sum_{l=1}^{L} I_l = K$. Suppose that measurement values v_m to v_n (v_m and

v_n are included) have been merged into the l^{th} bucket, and the new likelihood vector is presented as $\vec{p}_l = \{p_l^0, p_l^1\}$, after this merging, according to Eq. (3), where

$$p_l^j = (\sum_{\tau=m}^{n} c_{v_\tau}^j) / (\sum_{\tau=m}^{n} c_{v_\tau}^0 + \sum_{\tau=m}^{n} c_{v_\tau}^1) \quad , j=0, 1. \tag{4}$$

Hence, the original values v_m to v_n have to share the same likelihood vector $\vec{p}_l$. Obviously, it might cause some loss of the original information.

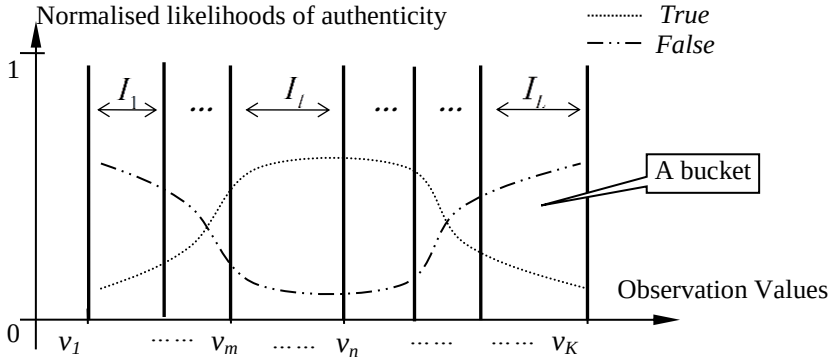

Figure 5 Information losses when merging a set of consecutive measurement values

The question is that if $\vec{p}_{v_m}, \cdots, \vec{p}_{v_n}$ are exactly the same as $\vec{p}_l$, this merging will cause no information loss; if $\vec{p}_{v_m}, \cdots, \vec{p}_{v_n}$ are different but close to $\vec{p}_l$, this merging can be considered as partially correct. Hence, the next issue is to quantify the differences or distances between vector $\vec{p}_l$ and each of $\vec{p}_{v_m}, \cdots, \vec{p}_{v_n}$.

3.2.3 Information loss modelling and discretisation optimisation

Many researchers have proposed methods to evaluate the distances or similarities between evidence. The following definition proposed by Jousselme *et al*. (2001) has been widely used:

$$d_{pba}(\vec{p}_1, \vec{p}_2) = \sqrt{\frac{1}{2}(\left\|\vec{p}_1\right\|^2 + \left\|\vec{p}_2\right\|^2 - 2 \cdot \left\langle \vec{p}_1, \vec{p}_2 \right\rangle)} \tag{5}$$

where $\left\|\vec{p}_1\right\|^2 = \left\langle \vec{p}_1, \vec{p}_1 \right\rangle$, and $\left\langle \vec{p}_1, \vec{p}_2 \right\rangle$ denotes the dot product operation of vectors $\vec{p}_1$ and $\vec{p}_2$. $d_{pba}(\vec{p}_1, \vec{p}_2) \in [0,1]$ can be considered as an *expected error rate* under the condition that the actual likelihood vector is $\vec{p}_1$, but the merged or reported one is $\vec{p}_2$.

Therefore, for the original observation value v_i in the l^{th} bucket, its *expected error rate* is denoted as $d_{pba}(\vec{p}_{v_i}, \vec{p}_l)$. Let $\rho(v_i)$ denote the density (probability of occurrence) of the original observation value v_i. Hence, the product of the *expected error rate* $d_{pba}(\vec{p}_{v_i}, \vec{p}_l)$ and the density $\rho(v_i)$ can be considered as an *expected information loss* when the observation value v_i has been merged into the l^{th} bucket. The densities of the original observation values $\{v_1, \cdots, v_K\}$ can be found in the verified samples, as in Table I. The $\rho(v_i)$ is presented as,

$$\rho(v_i) = (q^0_{v_i} + q^1_{v_i}) / (S^0 + S^1) \quad (6)$$

Then, the global *expected information loss* is the sum of all the *expected information losses* on original observation values $\{v_1, \cdots, v_K\}$. An optimal merging or discretisation on these values should keep the sum of information losses minimum. As mentioned, $\vec{p}_1$ denotes the merged likelihood vector of the l^{th} bucket, which contains I_l original measurement values. Since d_{pba} in Eq. (4) is denoted for the *expected error rate*, an appropriate $\{I_1, \cdots I_L\}$ can be solved in an optimisation, which is presented as,

$$\vec{I} = \{I_1, \cdots I_L\} = \arg\min \sum_{n=1}^{L} [\sum_{m=k_n}^{k_n + I_n - 1} d_{bpa}(\vec{p}_{v_m}, \vec{p}_n) \cdot \rho(v_m)] \quad (7)$$

where $k_n = \begin{cases} 1, n = 1 \\ \sum_{\xi=1}^{n-1} I_\xi, n > 1 \end{cases}$ and $\sum_{l=1}^{L} I_l = K$. Obviously, K ≥ L. Therefore, there are finite values of $\vec{I}$. Through enumerating all the possible values, $\vec{I}$ can be found. In practice, this algorithm is limited by the number of original measurement values, where *K* should be smaller than 100, otherwise this optimisation will be computationally intensive.

After merging, the buckets with different sizes can also be considered as new un-equal distance intervals, or an optimal discretisation on a node.

3.3 Step 3: BN inference with structure and parameters learning

After discretisation, the following problem is to build an inference framework whose formalization as described below.

BN is defined by a pair (S, Θ_s), where $S = (\chi, E)$ is a directed acyclic graph (DAG) with a set of nodes χ, and with a set of arcs or nodes $E = \{(X_i, X_j) \mid X_i, X_j \in \chi, X_i \neq X_j\}$ representing probabilistic dependencies among domain variables (Monti and Cooper, 1998). Θ_s represents the parameterization of a probability measure ρ defined over the space of possible instantiations of χ. Given a node $X_i \in \chi$, ***Pai*** is used to denote the set of parents of X_i in *S*. The essential property of BNs is summarized by the Markov property, and it assumes that each variable is independent of its non-descendants given its parents. The application of the chain rule, together with the Markov property, yields the following factorization of the joint probability of any particular instantiation $\vec{x}$ of all *n* variables:

$$\rho(\vec{x}) = \rho(x_1, \cdots, x_n) = \prod_{i=1}^{n} \rho(x_i \mid Pai, \Theta_S) \quad (8)$$

In this research, the authenticity (A) or the judgment of a blip can be described as two possible propositions or states {True (moving vessel), False (noise or stationary object)} as described previously. In an initial DAG, the velocity (D), direction (V), shape /slenderness (S), and authenticity (A) are formulated as nodes. It is worth mention that there are different kinds of objects in the False state, including shallows, rocks, noises, or even stationary vessels. It may be necessary to identify them in navigation and collision/grounding alert systems. In other words, there could be more states in the authenticity (A) node. For simplicity reasons, only the True and False states are considered in this research.

To address the problem of uncertainties, the structure of the DAG should be optimised or learned from verified data samples. There are several algorithms that can be applied, including the Bayesian Dirichlet equivalent scoring algorithm, K2 scoring algorithm (Cooper and Herskovits, 1991) and GS (Grow-Shrink) algorithm (Yang and Chang, 2002). Presently, the K2 scoring algorithm is widely accepted for constructing a BN from databases or records.

The principle of the K2 scoring algorithm is to assess the appropriateness of a structure based on verified records and the Dirichlet distribution. Under assumptions associated with lack of missing values, and independent parameters, the K2 scoring algorithm can be further simplified. Subsequently, the best scoring structure can be found using a hill-climbing heuristic algorithm. More detailed information about the K2 scoring algorithm can be found in the reference (Cooper and Herskovits, 1991). Presently, the K2 scoring algorithm is fully supported by the software tools of BN, including Netica, Hugin, and the MATLAB bnt toolbox.

Meanwhile, when the structure is determined, the conditional probability tables (CPTs) can be learned from verified samples. Usually, maximum likelihood estimation (MLE) is implemented to estimate CPTs if the training data is available. In this research, the expectation maximization (EM) algorithm is adopted, which is an iterative method to carry out MLE (Bilmes, 1998). It makes up for the disadvantage of traditional MLE methods that usually need to derive the analytical expressions of solutions (Peña *et al*., 2000). Such a process is also supported by the software tools mentioned above. Hence, the details of the EM algorithm will not be given here.

3.4 Step 4: Judgments based on a receiver operating characteristic (ROC) curve

Following the procedures above, the DAG for blip authenticity probability evaluation can be constructed. However, such probability values from the DAG do not directly lead to the final judgments on blips. In reality, noise blips will usually stay in the radar scan area for a long time; on contrary, moving vessels always pass through the waterway in a short period of time. In other words, there are far more noises than moving vessels in prior observations. The inferred probabilities of blips being moving vessels are probably much lower than 50%. The methodology proposed in this paper is required to make judgements on radar blips based on their inferred probability distributions. For example, a blip is regarded as a moving vessel with the likelihood of 75%, a noise with 25%. In this occasion, a threshold or a criterion should be obtained. If the probability of a blip being a moving vessel is larger than this threshold value, the blip is considered to be a true moving vessel; otherwise, it is considered as a noise or stationary object.

A receiver operating characteristic (ROC) can be used for the threshold optimisation. In statistics, a ROC curve is a graphical plot that illustrates the performance of a binary classifier system with different discrimination thresholds. Such a curve is created by plotting the true positive rate against the false positive rate at various threshold settings. In fact, a ROC curve can also be created by plotting false negatives rate against true negatives rate, which might be practical for collision/grounding alert systems. In this research, only the ROC curve plotting the true positive rate against the false positive rate is used for ease of the analysis. Some feature points such as inflection points are considered as optimal solutions (Hand and Till, 2011). In this research, as there are enough prior data, a more appropriate threshold can be learned from verified samples. The procedure of obtaining the threshold will be discussed in the case study.

4 A Case study

Overall, with a likelihood modelling, the intervals of blip graphic identities and inter-frame differences can be merged based on the minimization of expected information losses using Eq. (7). Based on this, a DAG for authenticity recognition can be constructed with structure and parameter learning. Eventually, final decisions will be made using a ROC curve. To validate the proposed methodology, a field testing was conducted in Yangtze River, Zhutuo County, Chongqing City, China from 11:55:36 to 16:05:35 on 11th January 2015.

4.1 Experimental platform and process

The photograph of the experiment platform is shown in Figure 6, and the testing radar is FAR2117S and installed on a wharf boat, which belongs to the local maritime administration. During the test, the radar provided 5,808 sequential radar images as illustrated in Figure 1, and 718 suspected moving vessel blips were captured. During the experiment period, there were actually only 42 moving vessels through manual verification. In four hours, there were 212,944 individual observations from these blips. However, only 8,143 observations were from moving vessels. As discussed in Section 3.4, the majority of observations were from noises or stationary objects.

It is worth mentioning that the waterway is only about 100 meters wide, thus the blips were validated by visual inspection.

Figure 6 Experiment radar at Zhutuo County, Yongchuan, Chongqing, China

For further validation of the proposed methodology, the verified samples have been divided into three sets by time. The samples from the first two hours are used to obtain the correlations between characteristics of blips and likelihoods of authenticity, which have been discussed in Section 3.1. Meanwhile, they are also used as the learning samples for the DAG. The samples from the third hour are used for obtaining an appropriate threshold in a ROC curve. Eventually, the verified objects in the last hour are used for validating the methodology.

4.2 Step 1: Inter-frame differences extraction of blips/objects

To implement the quantification methods of inter-frame differences described in Section 3.1, a software program was developed and presented in Figure 7. This program was built with VC++ in

Windows 7. As shown in Figure 7, radar images have already been overlapped on the S57 (A map format defined by the International Maritime Organization) electronic chart of the waterway. Three typical verified objects were notified as the red squares, and the enlarged images are shown on the top of the figure. They are noise objects No.17, No.27, and vessel object No.29. The white and orange circles are the objects' labels, which also mark the centres of the objects. Especially, the white dots are the trajectories of objects in former frames. Intuitively, a moving vessel object is different from a noise/stationary object in terms of the characteristics of velocity, direction, and shape.

Using the method proposed in Figure 4 and Section 3.1, such characteristics can be quantified.

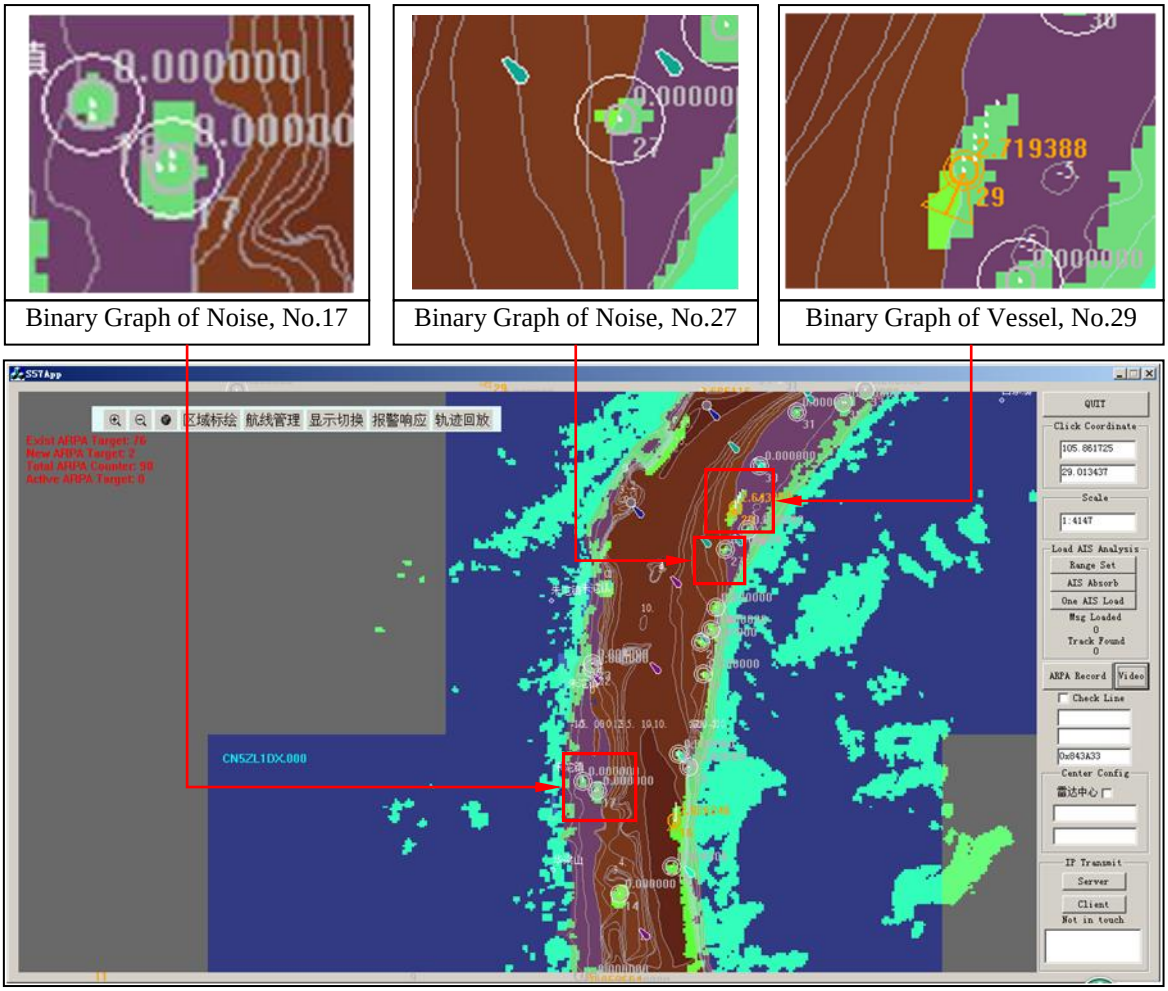

Figure 7 Experiment software based on VC++

All the blips in sequential images have been transformed to verified records with discrete attribute values, and these records are presented in a text form. A typical record is presented in Figure 8. As shown in this figure, a record contains several fields, which are separated by commas and represent different types of discrete attribute values. In this way, the course (direction), velocity, and slenderness are all stored in one record. Moreover, in this research, the vessel and noise/stationary records are saved separately.

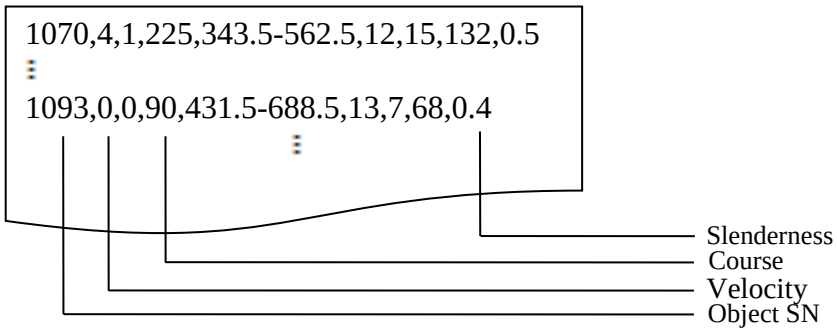

Figure 8 Text record definitions

4.3 Step 2: Node discretisation

The blip samples have been transformed to text forms, and the next step is to process them. As mentioned in Section 3.3, the discretisation of all the characteristics or nodes in a DAG are necessary in order to avoid a combinatorial explosion. Such discretisation is conducted as follows. In particular, the authenticity of a blip is denoted as two states: $\mathbf{A}_1$ (False, a noise or stationary object), $\mathbf{A}_2$ (True, a moving vessel).

In the following experiment, all the inference is processed using the bnt tool box (FullBNT_1.0.6) run in MATLAB 2013b. Detailed information about the bnt tool box can be found in the Google code website (Last access: 30th, Dec, 2015, https://code.google.com/p/bnt/).

- *Velocity*

The 100,893 verified samples from the first two hours are used to find the correlations between quantified values and likelihoods of authenticity based on Tables I, II, Eq. (2). For demonstration purposes, 20 of these verified samples are presented in Appendix A.1. Then, the vessel and noise velocity likelihoods of authenticity are presented in Figure 9, where the X axis represents the observation values of the velocity, and the Y axis represents the likelihoods of the states (True and False), or $c_{v_i}^j$ in Eq. (2). It is clear that the vessels are more likely to sail at 3 to 10 units (pixels), while the noise/stationary blips are more likely to move at lower than 2 units. It is logical that the noise blips are mostly drifting around a small area. In this figure, there are 13 original intervals in observation. As mentioned in Section 3.3, to reduce the complexity of the DAG, merging some observation values is necessary.

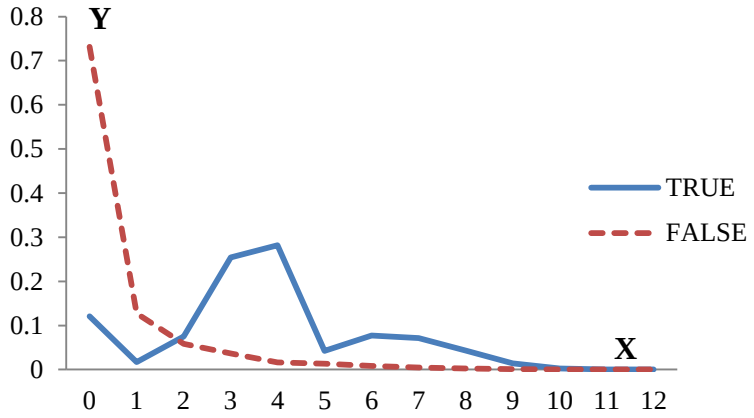

Figure 9 Velocity (D)-based normalised likelihoods of the states (True and False)

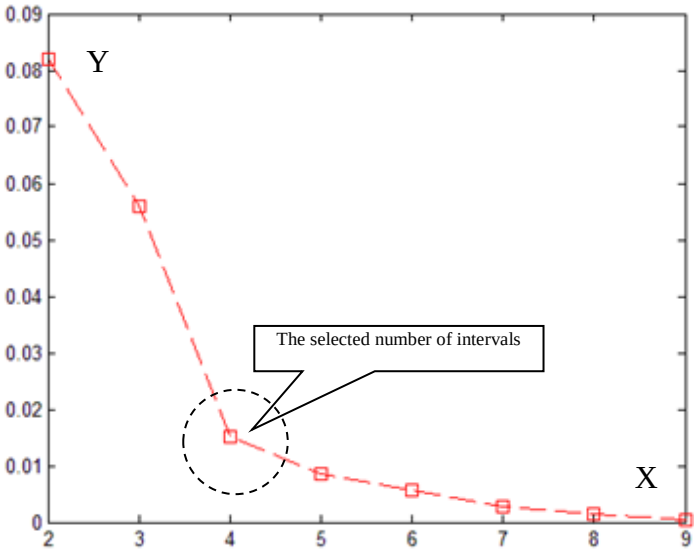

Figure 10 Velocity (D) intervals vs expected information loss

With the minimization of the expected losses in Eq. (7), the optimisation results are presented in Figure 10. In this figure, the X axis denotes the number of objective intervals, and the Y axis denotes the sum of the expected losses when optimal discretisation is satisfied, as described in Section 3.2. A computation example of the expected loss is presented in Appendix A.2. Having analysed the 100,893 verified samples in the first two hours, the expected losses in Figure 10 are generally presented as a concave curve. The inflection point on this curve can be considered as appropriate, and its corresponding value on the X axis is chosen as the number of objective intervals (Hand and Till, 2011; Nguyen and Sanner, 2013). In this occasion, the number of objective intervals is 4. It is worth noting that other optimisation methods can be introduced in the selection of the number of objective intervals. When the number of objective intervals is 4, based on Eq. (7), the optimal unequal distance intervals are presented as $\{\mathbf{D}_1, \mathbf{D}_2, \mathbf{D}_3, \mathbf{D}_4\} = \{\{0,1\}, \{2,3\}, \{4,5\}, \{6,7,8,9,10,11,12\}\}$.

- *Slenderness*

With the same verified samples, the slenderness likelihoods of authenticity are presented in Figure 11, where the X axis represents the intervals of slenderness, and the Y axis represents the likelihoods of the states (True and False). As the quotient of the pixel size to the circumcircle area, a slenderness value is continuous, meaning that there are infinite intervals. However, in the radar images, the pixel size of a blip is limited; as a result the interval of 0.1 is sufficient to describe it accurately. According to the figure, the moving vessel blips are more slender than the noise/stationary ones. In this figure, there are also 13 original intervals in the observations. Particularly, the blip size is based on how many pixels it occupies, and the value is denoted as an integer. The value of the circumcircle area is determined by the float's circumscribing circle of outermost edge points. Therefore, if a blip is too small, the size is possibly larger than the circumcircle area. In other words, the slenderness might be greater than 1.

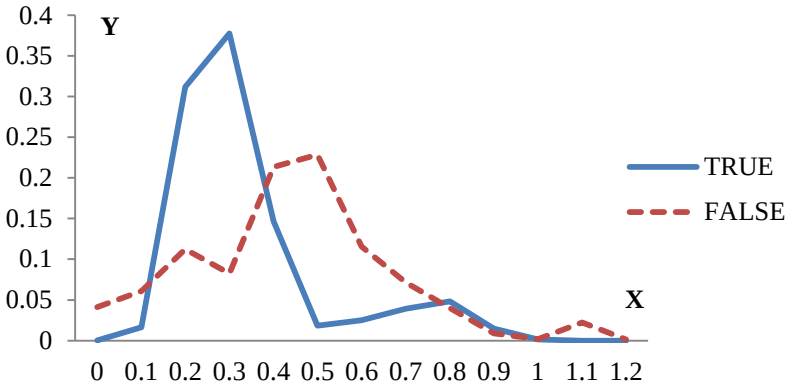

Figure 11 Shape/Slenderness (S)-based normalised likelihoods of the states (True and False)

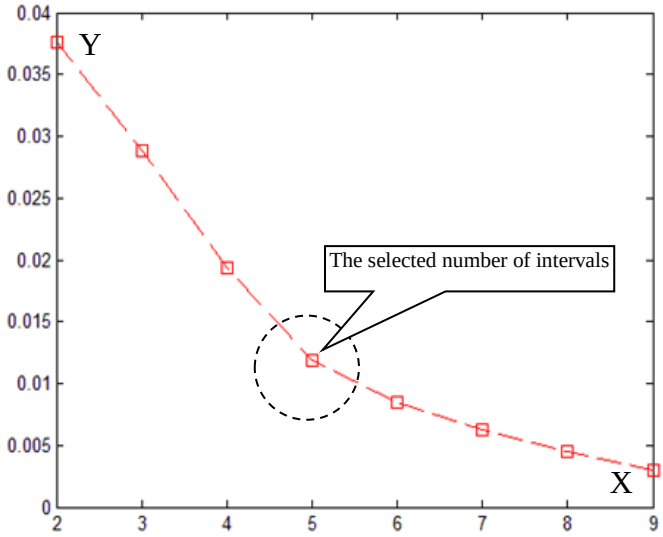

Figure 12 Shape (S) intervals merging vs expected loss

Just like the velocity (D), the optimisation results are presented in Figure 12. In this figure, the X axis denotes the number of objective intervals, and the Y axis denotes the sum of the expected information losses when optimal discretisation is satisfied, which is defined in Section 3.2 and Eq. (7). With the same principle as the velocity node (V), the number of objective interval number of shape evidence is selected as 5, and the optimal un-equal distance intervals are $\{\mathbf{S}_1, \mathbf{S}_2, \mathbf{S}_3, \mathbf{S}_4, \mathbf{S}_5\}$ = {{0,0.1,0.2}, {0.3,0.4}, {0.5,0.6}, {0.7,0.8,0.9}, {1.0,1.1,1.2}}.

- *Direction*

The direction is different from the velocity and slenderness. Since the radar images have been pixelated and transformed to the binarization form, the blip is probably drifting around a small area when its values crowd on 0, 45, 90, 135, 180, 225, 270 or 315 degrees, and is more likely to be a noise target as shown in Figure 13. In this figure, the X axis denotes the angle; the Y axis denotes the normalised likelihoods of the states (True and False). As discussed in Section 3.2, when the number of intervals is large, the proposed merging method will take a long time. Therefore, the proposed optimisation in Eq. (7) is not appropriate in this node. Nevertheless, the pattern will be easily recognized using a simple principle, and all the intervals can be simplified to two sets $\{\mathbf{V}_1$ (noise of stationary object), $\mathbf{V}_2$ (moving vessel)$\}$ = {{45, 90, 135, 225, 270, 315}, $\mathbf{V}$-$\mathbf{V}_1$}, where $\mathbf{V}$ denotes all the possible direction values. Special attention needs to be paid to the fact that there are not many

observations with 0 or 180 degree from noise samples. Therefore, 0 and 180 degree are not included in set $\mathbf{V}_1$.

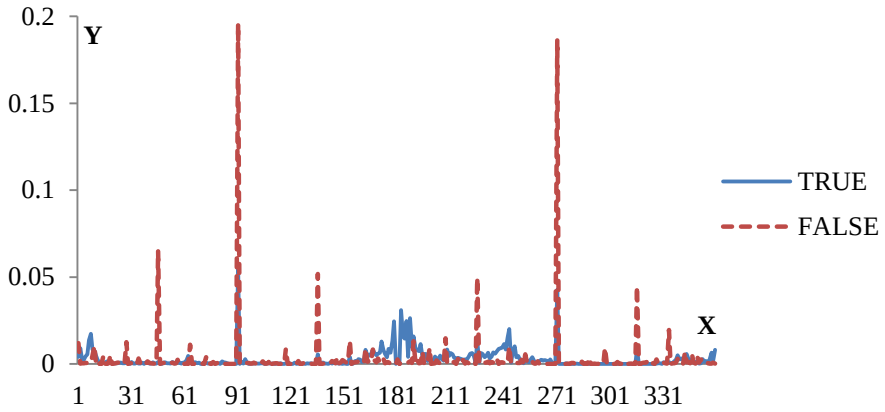

Figure 13 Direction (V)-based normalised likelihoods of the states (True and False)

4.4 Step 3: DAG updating using the K2 algorithm

After discretisation, a BN can be used to infer the authenticity of a blip. At the very beginning, an initial DAG has to be established based on the expert judgments on how the authenticity (A) is influenced by the velocity (D), direction (V), and slenderness (S). In fact, slenderness (S) is influenced by velocity (D) considering the fact that the faster an object moves, the more slender its blip is. Direction (V) is also influenced by velocity (D) given that when an object moves slowly, it is more likely for the blip drifting around a small area to have its course/direction on 45, 90, 135, 215, 270 or 315 degrees. Therefore, the initial DAG obtained through investigating the causal and dependent relationships between D, V, S and A is presented in Figure 14.

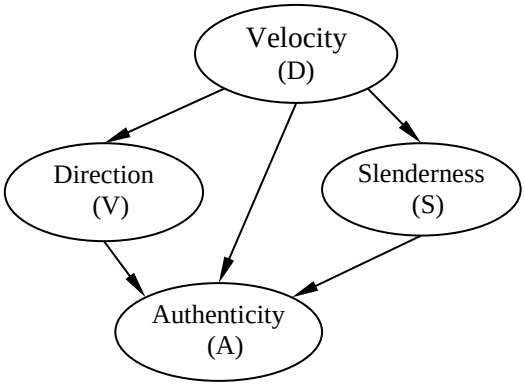

Figure 14 Initial DAG for authenticity recognition before learning

However, as discussed in Section 3.2, the DAG might not be the best reflection of the relationships among Velocity (D), Direction (V), Slenderness (S), and Authenticity (A). The samples collected from the first two hours of the experiment are used for improving the structure. With the help of the K2 scoring algorithm, an improved DAG structure can be constructed. Such a procedure is implemented with the 'learn_struct_K2' function in the MATLAB 2013b bnt toolbox, and the output is presented as Figure 15 where the nodes named 1, 2, 3 and 4 denote the Velocity (D), Direction (V), Slenderness (S), and Authenticity (A) respectively. Hence, the updated DAG structure is shown in Figure 16. From the new DAG, Direction (V) also has direct influence on Slenderness (S).

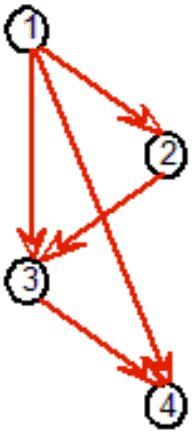

Figure 15 The output of the 'learn_struct_K2' function in MATLAB 2013b

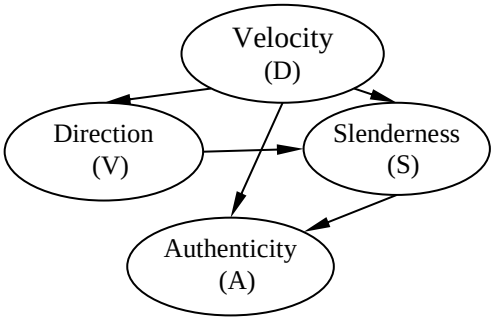

Figure 16 Upgraded DAG after learning using the K2 scoring algorithm

Subsequently, the CPT of each node can be learned using the EM algorithm and the verified samples from first two hours of the experiment as mentioned in Section 3.3. Such a procedure is supported by the 'learn_params' in MATLAB 2013b bnt toolbox. The CPTs for all the nodes are presented as Table III to Table VI. Eventually, the formulated DAG in Figure 16 will be used to reason the authenticity of blips in observations.

Table III. The CPT of node Velocity (D)

$\mathbf{D}_1$	$\mathbf{D}_2$	$\mathbf{D}_3$	$\mathbf{D}_4$
0.8318	0.1023	0.0418	0.0241

Table IV. The CPT of node Direction (V)

	$\mathbf{V}_1$	$\mathbf{V}_2$
$\mathbf{D}_1$	0.6997	0.3003
$\mathbf{D}_2$	0.0867	0.9133
$\mathbf{D}_3$	0.0396	0.9604
$\mathbf{D}_4$	0.0156	0.9844

Table V. The CPT of node Slenderness (S)

	$\mathbf{S}_1$		$\mathbf{S}_2$		$\mathbf{S}_3$		$\mathbf{S}_4$		$\mathbf{S}_5$	
	$\mathbf{V}_1$	$\mathbf{V}_2$	$\mathbf{V}_1$	$\mathbf{V}_2$	$\mathbf{V}_1$	$\mathbf{V}_2$	$\mathbf{V}_1$	$\mathbf{V}_2$	$\mathbf{V}_1$	$\mathbf{V}_2$
$\mathbf{D}_1$	0.1859	0.2603	0.2601	0.2985	0.3617	0.3441	0.1557	0.086	0.0365	0.0111
$\mathbf{D}_2$	0.3072	0.2038	0.4153	0.4782	0.2267	0.2519	0.0508	0.0605	0	0.0056
$\mathbf{D}_3$	0.2273	0.1859	0.3864	0.6142	0.3068	0.1592	0.0795	0.0389	0	0.0019
$\mathbf{D}_4$	0.75	0.73	0.1000	0.1750	0.15	0.0578	0	0.0253	0	0.0119

Table VI. The CPT of node Authenticity (A)

	$\mathbf{A}_1$ (False)	$\mathbf{A}_2$ (True)

	S_1	S_2	S_3	S_4	S_5	S_1	S_2	S_3	S_4	S_5
D_1	0.9978	0.9987	0.9971	0.968	0.9984	0.0022	0.0013	0.0029	0.032	0.0016
D_2	0.8999	0.7926	0.975	0.9662	1	0.1000	0.2074	0.025	0.0338	0
D_3	0.6595	0.5884	0.9918	0.9556	1	0.3405	0.4116	0.0082	0.0444	0
D_4	0.5411	0.8969	0.9868	0.9688	1	0.4589	0.1031	0.0132	0.0313	0

4.5 Step 4: Final judgments using the authenticity probability and a ROC curve

For a blip, the probabilities of the True state will be evaluated using the above procedures. The next step is to find an optimal threshold probability value for a final judgment and to determine whether this blip is a real moving vessel.

As described in Section 4.1, the samples from the third hour are used for training the threshold value. First, the authenticity probabilities of these verified samples can be reasoned by the DAG. Subsequently, the 'plotroc' function in MATLAB 2013b can be used to plot these verified samples for formulating a ROC curve, which is presented in Figure 17. As discussed previously, the ROC curve can also be created by plotting false negatives rate against true negatives rate for other applications.

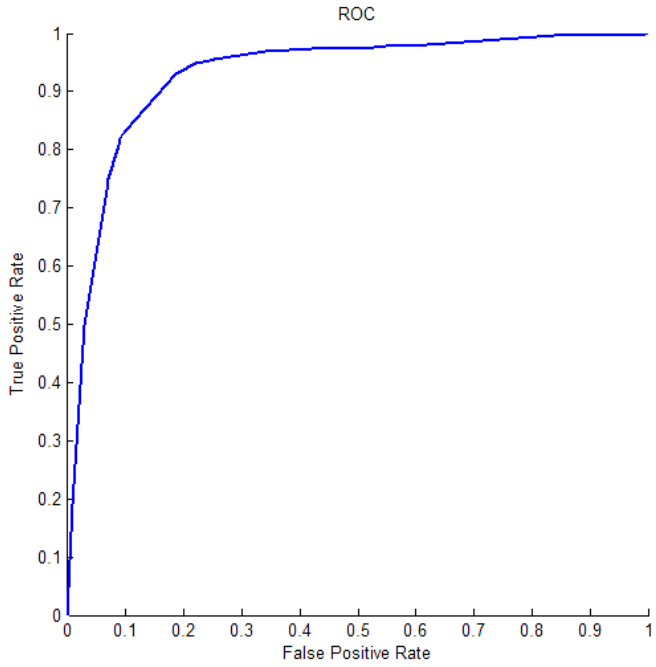

Figure 17 ROC curve on result

Then, there are 23 recommended threshold values (England, 1988) offered by this 'plotroc' function based on statistical characteristics. Eventually, an optimal threshold can be determined in accordance with a particular objective. In this research, the objective is to maximize the global accuracy. Let t denote the threshold value, and an optimal threshold value t^* can be presented as,

$$t^* = \arg\max\left(\sum_{p=1}^{P} \mathrm{sgn}(B(V_p) - t) + \sum_{q=1}^{Q} \mathrm{sgn}(t - B(N_q))\right) \quad (9)$$

where $\begin{cases} \mathrm{sgn}(x) = 1, x > 0 \\ \mathrm{sgn}(x) = 0, x = 0 \\ \mathrm{sgn}(x) = -1, x < 0 \end{cases}$, $\{V_1, \cdots, V_p, \cdots, V_P\}$ denote the P observations from the verified vessels, $\{N_1, \cdots, N_q, \cdots, N_Q\}$ denote the Q observations from the noise or stationary objects. $B(V_p)$ is the probability that observation V_p was from a moving vessel; $B(N_q)$ is the probability that N_q

observation was from a moving vessel. Both $B(V_p)$ and $B(N_q)$ are calculated using the formulated DAG shown in Figure 16 and the CPTs in Tables III~VI. The possible values of *t* can be obtained through the ROC function ('roc' and 'plotroc') in MATLAB 2013b.

Using Eq. (9), the threshold is obtained as 0.0373. Therefore, if the probability of a blip being a moving vessel is larger than this threshold value, the blip is considered to be a true moving vessel. It is worth noting that the threshold value is usually low as described in Section 3.4. In the observations of this research, the number of noises is much larger than that of real moving vessels.

With the threshold value, the samples of the last hour in the experiment are used for a global validation. For these verified samples, the probabilities of authenticity are reasoned by the DAG, and the judgements are determined using the threshold value 0.0373. Eventually, the result is presented in Table VII.

Table VII Results of analysis of the verified samples in last hour using the developed model

	Total	Correct identification	In-correct identification	Accuracy
Moving vessel	2,035	1,692	343	83.14%
Noises or stationary objects	51,201	46,120	5,081	90.08%
Overall				90.03%

This table shows the results obtained from the developed model. From Table VII, it can be seen that there are 2,035 verified observations of being moving vessels and 51,201 verified observations of being noises or stationary objects in the analysis. The developed model produced 1,692 correct identifications out of 2,035 moving vessel observations, leading to the recognition accuracy of 83.14%. As for the 51,201 verified observations of being noises or stationary objects, the model produces a recognition accuracy of 90.08%. In total, the global accuracy reached 90.03%.

When the threshold is unknown, the ROC curve of the samples in the last hour is presented in Figure 18.

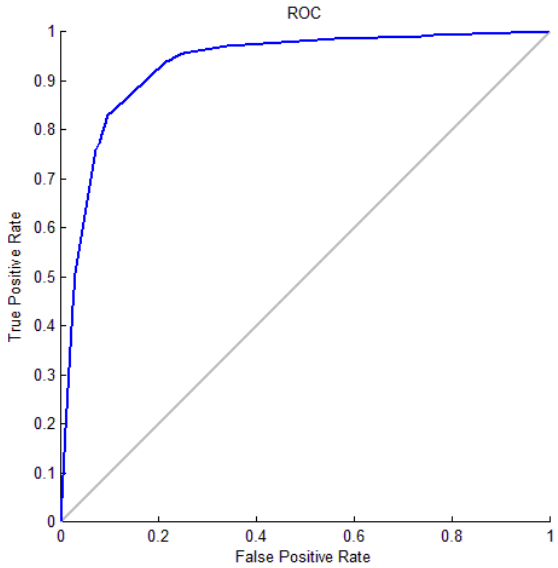

Figure 18 The ROC curve of the samples in the last hour

Particularly, incorrect identifications might be a threat to safety in collision/grounding alert systems. In fact, consecutive incorrect identifications are rare on any particular object using the

methodology. More accurate identification on an object can be implemented from the analysis of more consecutive frames, which may need to be further analysed in the future research.

4.6 Comparisons with other classifiers

For comparison purposes, the research introduces three kinds of classifiers, namely logistic regression, fuzzy c-means (FCM) (Ma *et al.*, 2015), and error back-propagation (BP) based artificial neural networks (ANN) to process the same samples.

Logistic regression is a common binary classifier in medical sciences (Rasmussen *et al.*, 2014). It measures the relationship between target attributes and patterns by estimating probabilities using a logistic function. The velocity, course, and slenderness quantified in Section 4.2 can be used as the attributes. The detailed formulation of logistic regression can be found in Rasmussen *et al.* (2014). The same samples of the first two hours can be used to train the coefficients of the logistic function. Particularly, this procedure can be implemented with the 'glmfit' command of MATLAB 2013b. Subsequently, the probabilities about the two patterns can be inferred with the 'glmval' function. Generally, 0.5 is used as a threshold in logistic regression (Rasmussen *et al.*, 2014) in judgements. In this occasion, the classification result is presented in Table IX, and the proposed methodology is more accurate than logistic regression in this application.

Table IX Results of analysis of the verified samples in last hour using logistic regression

	Total	Correct identification	In-correct identification	Accuracy
Moving vessel	2,035	1,738	297	85.42%
Noises or stationary objects	51,201	43,603	7,598	85.16%
Overall				85.17%

Without any inference and discrete models, FCM is capable of classifying a dataset to objective number subsets. In principle, FCM is based on the distribution of data in a vector space. Hence, a three dimensional space has to be defined first. In this space, the X-axis represents the normalised velocity (D), the Y-axis represents the normalised direction (V), and the Z-axis represents the normalised slenderness (S). Subsequently, a blip with three attributes quantified in Section 4.2 can be denoted as a vector or a coordinate $\{D, V, S\}$ in such a space. Then, FCM can be introduced to classify all the blips in this space into two sub-sets and the detailed procedures can be found in Ma *et al.* (2015). The result of FCM is presented in Table VIII. Obviously, the BN-based methodology proposed in this research is also superior to the FCM classifier in this application.

Table VIII Results of analysis of the verified samples in last hour using FCM

	Total	Correct identification	In-correct identification	Accuracy
Moving vessel	2,035	1,548	487	76.06%
Noises or stationary objects	51,201	36,649	14,552	71.58%
Overall				71.75%

The BP-based ANN is another popular algorithm in un-supervised machine learning applications (Bishop, 1995; Schmidhuber, 2015). For simplicity reasons, the neural pattern recognition tool (nprtool) of MATLAB 2013b is used to implement the BP-based classification (KrishnaSri *et al.*, 2016). Generally, the element number of the hidden layer of ANN is set to be 2 times of the number of the input elements (velocity, course, and slenderness) (Jamli *et al.*, 2015), or 6 in this research. The

same samples of the first two hours are used for training the ANN, and the ones from the last hours are used for validation. Particularly, a ROC curve is needed here since there is no conventional threshold value in an ANN model. Eventually, the classification ROC curve of the validation samples is given in Figure 19 with the help of "nprtool" of MATLAB 2013b. In this figure, the ROC curve of the BP-based ANN model is presented as a blue solid line, and the one of the proposed methodology is presented as a red dash line. The highest overall identification accuracy on moving vessels and noises/ stationary objects through the use of the BP-based ANN is 96.34% when the threshold is 0.045. The detailed recognition result is presented in Table X. In particular, the recognition accuracy on real moving vessels is only 65.06%. Given the significance of identifying moving vessels from the blips on a radar screen, the recognition process is less impressive in this occasion. The BN-based methodology is superior to the BP-based ANN in this application.

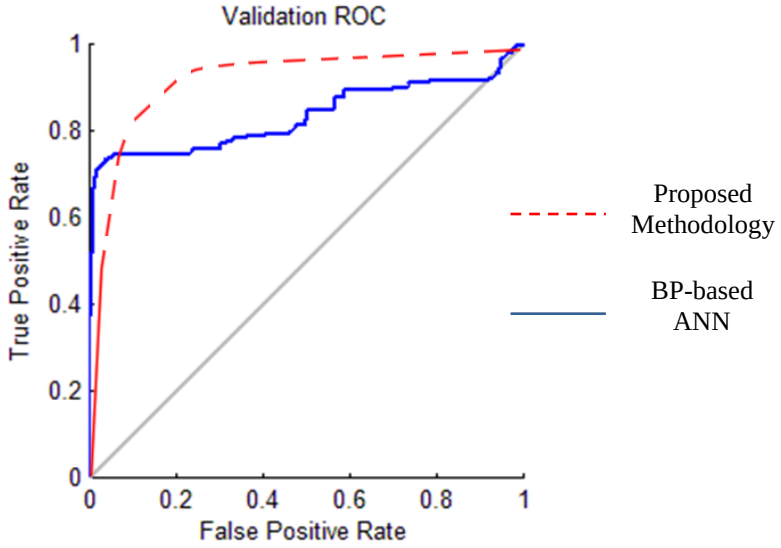

Figure 19 The output of neural pattern recognition tool

Table IX Results of analysis of the verified samples in last hour using BP-based ANN

	Total	Correct identification	In-correct identification	Accuracy
Moving vessels	2,035	1,324	711	**65.06%**
Noises or stationary objects	51,201	49,962	1,239	97.58%
Overall				96.34%

5 Conclusions

Marine radar is the kernel sensor in the management and avoidance of collision. The study proposed a BN-based identification methodology for identifying moving vessels from blips in radar images. The conclusions are given as follows:

1) Referring to manual work, this methodology is based on original sequential radar images which contain sufficient information for further recognition. Different from traditional filtering algorithms, it does not need to make any assumption on objects' states.
2) With the inter-frame differences in frames, the BN-based methodology incorporating the velocity, course and shape of blips is capable of updating the structure and parameters from verified samples. The attribute value intervals can be merged based on the likelihood vector distances and the minimization of expected information losses. The judgments can be made through a ROC curve, achieving high classification accuracy.

3) In future study, the quantification of radar blip attributes may be conducted in fewer frames to improve the recognition speed. Identification of specific objects such as rocks and shoals from background noises may also prove useful.
4) The continuities of blips may need to be introduced into the conjunctive inference, which might further improve the classification accuracy. It may also be desirable to develop an interactive optimisation model in response to the feedback from radar operators, in order to achieve improved accuracy of identifying moving vessels from blips on a real time basis.

The proposed methodology can also be used in situations where the behaviours of moving vessels need to be further investigated for safety and security reasons.

Acknowledgements

Thanks for financial support are given to National Science Foundation of China (Grant no. 61503289 and 51479158), EU (Marie Curie grant REFERENCE – 314836), and Innovation Groups Project of Hubei Province Natural Science Foundation (No: 2013CFA007).

Appendix

A.1

As described, there are 100,893 verified samples which have been captured in the first two hour. These samples are saved as a text form presented in Section 4.2 and Figure 8. It is worth mentioning that there are about 10 to 100 records for a blip, as it usually stay in the observation area for about 20 to 300 seconds. To make it more visualised, several verified samples in the text form are presented as follows.

10 observations from verified vessel blips are presented as:

178,12,4,135,549.5-479.5,5,11,33,0.3
178,12,4,135,549.5-479.5,5,11,33,0.3
301,0,0,240,629.0-611.0,16,8,81,0.3
301,10,3,246,589.5-597.5,15,9,72,0.3
770,14,4,244,590.5-592.0,19,10,86,0.2
770,9,3,214,518.5-534.0,3,4,12,0.6
962,0,0,270,624.5-610.5,13,7,74,0.4
962,5,2,270,624.0-610.5,14,7,74,0.4
1206,8,8,338,564.0-296.5,6,13,59,0.4
1206,9,8,338,563.5-297.5,7,15,62,0.3

10 observations from verified noise blips are presented as:

0,1,0,225,533.0-181.5,23,10,94,0.2
0,1,0,225,533.0-181.5,23,10,94,0.2
1,0,0,0,521.0-189.5,10,9,56,0.4
1,1,0,90,521.0-189.5,10,9,55,0.4
1524,1,0,270,571.0-512.0,38,106,343,0.0
1524,0,0,270,571.5-512.0,39,106,343,0.0
2086,5,2,355,517.0-312.5,6,3,25,0.7
2086,6,2,355,517.0-312.5,6,3,25,0.7
2837,4,1,300,559.5-286.5,9,7,28,0.3

2837,4,1,326,561.0-287.5,6,9,25,0.3

A.2

The expected loss is defined as Eq. (7),

$$\vec{I} = \{I_1, \cdots I_L\} = \arg\min \sum_{n=1}^{L} [\sum_{m=k_n}^{k_n+I_n-1} d_{bpa}(\vec{p}_{v_m}, \vec{p}_n) \cdot \rho(v_m)] \quad (7)$$

There are 13 original intervals in the velocity observations. These intervals are presented as $\{v_1, \cdots, v_{13}\} = \{0,1,\cdots,12\}$. Suppose L = 4, the objective is to merge these intervals into L = 4 buckets. According to Eq. (6) and Table I, $\{\rho(v_1), \cdots, \rho(v_{13})\}$ = {0.12059, 0.01730, 0.07519, 0.25390, 0.28153, 0.04276, 0.07735, 0.07134, 0.04324, 0.01417, 0.00240, 0.00024, 0.00000}. The normalised likelihoods of authenticity $\vec{p}_{v_m}, \vec{p}_n$ can be solved with Table II and Eq. (4). Afterwards,

$$\vec{I} = \{I_1, I_2, I_3, I_4\} = \arg\min \sum_{n=1}^{4} [\sum_{m=k_n}^{k_n+I_n-1} d_{bpa}(\vec{p}_{v_m}, \vec{p}_n) \cdot \rho(v_m)] \quad (10)$$

where $k_n = \begin{cases} 1, n = 1 \\ \sum_{\xi=1}^{n-1} I_\xi, n > 1 \end{cases}$. Since $I_1 + I_2 + I_3 + I_4 = 13$ and they are integers, all the possible $\vec{I}$ can be enumerated. Using Eq. (10), $\vec{I} = \{I_1, I_2, I_3, I_4\} = \{2, 2, 2, 7\}$, which denotes that the optimal 4 buckets contain 2, 2, 2, and 7 original observation intervals. Therefore, the buckets are presented as {$\mathbf{D}_1$, $\mathbf{D}_2$, $\mathbf{D}_3$, $\mathbf{D}_4$} = {{0,1}, {2,3}, {4,5}, {6,7,8,9,10,11,12}}. By this moment, $\sum_{n=1}^{4} [\sum_{m=k_n}^{k_n+I_n-1} d_{bpa}(\vec{p}_{v_m}, \vec{p}_n) \cdot \rho(v_m)]$ or the expected loss equals to 0.056.

References

Bacardit, J. & Garrell, J. M. (2003). Evolving multiple discretisations with adaptive intervals for a pittsburgh rule-based learning classifier system. In Genetic and Evolutionary Computation—GECCO 2003, 1818-1831.

Bilmes, J. A. (1998). A gentle tutorial of the EM algorithm and its application to parameter estimation for Gaussian mixture and hidden Markov models. International Computer Science Institute, 4(510), 126.

Bishop, C. M. (1995). Neural networks for pattern recognition. Oxford university press.

Carvalho, E. A., Ushizima, D. M., Medeiros, F. N., Martins, C. I. O., Marques, R. C. & Oliveira, I. N. S. (2010). SAR imagery segmentation by statistical region growing and hierarchical merging. Digital Signal Processing, 20(5), 1365-1378.

Chen, W. (2015). Spatial and temporal features selection for low-altitude target detection. Aerospace Science & Technology, 40, 171–180.

Chin, H. C. & Debnath, A. K. (2009). Modeling perceived collision risk in port water navigation. Safety Science, 47(10), 1410-1416.

Clarke, E. J. & Barton, B. A. (2000). Entropy and MDL discretisation of continuous variables for Bayesian belief networks. International Journal of Intelligent Systems, 15(1), 61-92.

Cooper, G. F. & Herskovits, E. (1991). A Bayesian method for constructing Bayesian belief networks from databases. In Proceedings of the Seventh conference on Uncertainty in Artificial Intelligence, 86-94.

De Feo, M., Graziano, A., Miglioli, R., & Farina, A. (1997). IMM-JPDA versus MHT and kalman filter with NN correlation: performance comparison. Radar, Sonar and Navigation, IEE Proceedings -, 144(2), 49-56.

Dempster, A. P. (1967). Upper and lower probabilities induced by a multivalued mapping. *The annals of Mathematical Statistics*, 38(2), 325-339.

England, W. L. (1988). An exponential model used for optimal threshold selection on ROC Curues. Medical Decision Making, 8(2), 120-131.

Farrell, W. J. (2008). Interacting multiple model filter for tactical ballistic missile tracking. IEEE Transactions on Aerospace and Electronic Systems, 44(2), 418-426.

Goerlandt, F., Montewka, J., Kuzmin, V. & Kujala, P. (2015). A risk-informed ship collision alert system: framework and application. Safety Science, 77, 182-204.

Goerlandt, F. & Montewka, J. (2014). A probabilistic model for accidental cargo oil outflow from product tankers in a ship-ship collision. Marine Pollution Bulletin, 79(1-2), 130-144.

Grünwald, P. (2000). Model selection based on minimum description length. Journal of Mathematical Psychology, 44(1), 133-152.

Hand, D. J. & Till, R. J. (2001). A simple generalisation of the area under the ROC curve for multiple class classification problems. Machine learning, 45(2), 171-186.

He, X., Bi, Y. & Guo, Y. (2015). Target Tracking Algorithm of Ballistic Missile in Boost Phase Based on Ground-based Radar Systems. Journal of Information & Computational Science 12(2), 855–864.

Hänninen, M. & Kujala, P. (2014). Bayesian network modeling of port state control inspection findings and ship accident involvement. Expert Systems with Applications, 41(4), 1632–1646.

IEC, I. 62388 (2013): Maritime navigation and radio-communication equipment and systems. Shipborne radar. Performance requirements, methods of testing and required test results.

Jamli, M. R., Ariffin, A. K. & Wahab, D. A. (2015). Incorporating feedforward neural network within finite element analysis for L-bending springback prediction. Expert Systems with Applications, 42(5), 2604-2614.

Jousselme, A. L., Grenier, D. & Bossé, É. (2001). A new distance between two bodies of evidence. Information fusion, 2(2), 91-101.

Kotsiantis, S. & Kanellopoulos, D. (2006). Discretisation techniques: A recent survey. GESTS International Transactions on Computer Science and Engineering, 32(1), 47-58.

Kosuge, Y., Kameda, H. & Mano, S. (1997). Kalman Filter and α - β filters for radar tracking. Electronics and Communications in Japan (Part I: Communications), 80(3), 67-77.

KrishnaSri, D., Suja, P. & Tripathi, S. (2016). Emotion Recognition from 3D Images with Non-Frontal View Using Geometric Approach. In Advances in Signal Processing and Intelligent Recognition Systems, 63-73.

Li, B. & Pang, F. W. (2013). An approach of vessel collision risk assessment based on the D–S evidence theory. Ocean Engineering, 74, 16-21.

Ma, F., Wu, Q., Yan, X., Chu, X. & Zhang, D. (2015). Classification of automatic radar plotting aid targets based on improved fuzzy C-Means. Transportation Research Part C: Emerging Technologies, 51, 180-195.

Mazaheri, A., Goerlandt, F. & Kujala, P. (2012). A decision support tool for VTS centers to detect grounding candidates. Transnav the International Journal on Marine Navigation & Safety of Sea Transportation, 7 (3), 337-343.

Montewka, J., Goerlandt, F., Kujala, P. & Lensu, M. (2015). Towards probabilistic models for the prediction of a ship performance in dynamic ice. Cold Regions Science & Technology, 112, 14-28.

Monti, S. & Cooper, G. F. (1998). A multivariate discretisation method for learning Bayesian networks from mixed data. In Proceedings of the 14th Conference on Uncertainty in Artificial Intelligence, 404-413.

Nam, B. W., Lee, K. H., Lee, J. M., Kim, D. S., Ku, B. J. & Li, R.(2015). A study on the estimation method of risk based area for jetty safety monitoring. Sustainability, 7(10), 13154-13168.

Nguyen, T. & Sanner, S. (2013). Algorithms for direct 0--1 loss optimisation in binary classification. In Proceedings of the 30th International Conference on Machine Learning, 1085-1093.

Peña, J. M., Lozano, J. A. & Larrañaga, P. (2000). An improved Bayesian structural EM algorithm for learning Bayesian networks for clustering. Pattern Recognition Letters, 21(8), 779-786.

Ranjani, J. J. & Thiruvengadam, S. J. (2012). Fast Threshold Selection Algorithm for Segmentation of Synthetic Aperture Radar Images. Radar, Sonar & Navigation, IET, 6(8), 788-795.

Rasmussen, M. A., Maslova, E., Halldorsson, T. I. & Olsen, S. F. (2014). Characterization of dietary patterns in the danish national birth cohort in relation to preterm birth. Plos One, 9(4), e93644.

Riveiro, M., Falkman, G. & Ziemke, T. (2008). Visual analytics for the detection of anomalous maritime behaviour. In Proceedings of Information Visualisation Conference, 273-279.

Schmidhuber, J. (2015). Deep learning in neural networks: An overview. Neural Networks, 61, 85-117.

Shafiei, M. H. & Binazadeh, T. (2015). Application of neural network and genetic algorithm in identification of a model of a variable mass underwater vehicle. Ocean Engineering, 96, 173-180.

Simsir, U., Amasyalı, M. F., Bal, M., Çelebi, U. B. & Ertugrul, S. (2014). Decison support system for collision avoidance of vessels. Applied Soft Computing, 25, 369–378.

Vicen-Bueno, R., Carrasco-Álvarez, R., Rosa-Zurera, M. & Nieto-Borge, J. C. (2009). Sea clutter reduction and target enhancement by neural networks in a marine radar system. Sensors, 9(3), 1913-1936.

Xu X.B., Zhou Z. & Wang, C.L. (2013). Data fusion algorithm of fault diagnosis considering sensor measurement uncertainty. International Journal on Smart Sensing and Intelligent System, 6(1), 171-190.

Yang, J. B. & Xu, D. L. (2014). A Study on Generalising Bayesian Inference to Evidential Reasoning. In Belief Functions: Theory and Applications, 180-189.

Yang, S. & Chang, K. C. (2002). Comparison of score metrics for Bayesian network learning. IEEE Transactions on Systems, Man and Cybernetics, Part A: Systems and Humans, 32(3), 419-428.

Yoo, J. C. & Kim, Y. S. (2003). Alpha–beta-tracking index (α–β–Λ) tracking filter. Signal Processing, 83(1), 169-180.

Zhai, S. & Jiang, T. (2014). Target detection and classification by measuring and processing bistatic UWB radar signal. Measurement, 47, 547-557.

Zhang, D., Yan, X. P., Yang, Z. L., Wall, A. & Wang, J. (2013). Incorporation of formal safety assessment and Bayesian network in navigational risk estimation of the Yangtze River. Reliability Engineering & System Safety, 118, 93-105.

Zhao, H. Y., Quan, W., Weiwei, W., Qingping, W., Shenghai, J. & Naichang, Y. (2014). Hierarchical vessel classifier based on multifeature joint matching for high-resolution inverse synthetic aperture radar images. Journal of Applied Remote Sensing, 8(1), 083563-083563.

Zhou, D., Shen, X. & Yang, W. (2013). Radar target recognition based on fuzzy optimal transformation using high-resolution range profile. Pattern Recognition Letters, 34(3), 256-264.